Supporting Information

In-Situ Constructing Polyether-Based Composite Electrolyte with Bi-Phase Ion Conductivity and Stable Electrolyte/Electrode Interphase for Solid-State Lithium Metal Batteries

Shujun Zheng[a], Yuyang Chen[a], Kai Chen[a], Shengyuan Yang[a], Roohollah Bagherzadeh[c], Yue-E Miao[a,*], and Tianxi Liu[a,b]

[a] *State Key Laboratory for Modification of Chemical Fibers and Polymer Materials, College of Materials Science and Engineering, Donghua University, Shanghai, 201620, China*

[b] *Key Laboratory of Synthetic and Biological Colloids, Ministry of Education, School of Chemical and Material Engineering, Jiangnan University, Wuxi, 214122, China*

[c] *Advanced Fibrous Materials LAB, Institute for Advanced Textile Materials and Technologies (ATMT), School of Advanced Materials and Processes, Amirkabir University of Technology, Tehran, Iran*

* *Corresponding author.*
E-mail address: yuee_miao@dhu.edu.cn (Y. E. Miao).

This file includes:

Experimental Section

Fig. S1 to S12.

Experimental Section

Preparation of the ceramic nanofiber electrolyte

The $La_{0.56}Li_{0.33}TiO_3$ (LLTO) ceramic nanofiber electrolyte was prepared by electrospinning and solid-state sintering method. Stoichiometric amount of lithium nitrate, n-propyl zirconate, tetrabutyl titanate, and lanthanum nitrate hexahydrate were dissolved in a mixed solution of acetic acid and *N,N*-dimethylformamide. Next, 10 wt% of PVP was added to the above mixed solution and continuously stirred for 12 h until a yellow transparent precursor solution was obtained. To control the thickness of the flexible nanofiber membrane at approximately 200 μm, the above solution was transferred into a 10 mL syringe and electrospun for 7.5-8 h. The detailed parameters were set as follows: the distance between the needle tip and the collector was fixed at 15 cm, and the injection speed was 0.08 mm min^{-1} combine with a voltage of 13 kV. Then, the collected flexible nanofiber membrane was placed into an alumina boat for sintering. The product was first calcined at 600 °C for 2 h with a heating rate of 5 °C min^{-1}, and then kept at 800 °C for 2 h in air to obtain the embedded LLTO nanofiber frame with a thickness of ≈150 μm (Fig. S4). Subsequently, the LLTO electrolyte was pressed into a 12 mm slice for battery assembly.

Preparation of the polyether-based composite electrolyte

Electrolyte preparation and battery assembly were carried out in a glove box filled with argon gas, in which the content of O_2 and H_2O were below 0.01 ppm. Before the experiment, the Li foil was treated as a sacrificial component in the 1,3-dioxolane (DOL) solvent for 24 h, which would react with any traces of water to chemically dry DOL. Subsequently, LiTFSI and $Al(OTf)_3$ were added into the DOL solvent, respectively, and vigorously stirred to obtain a 2 M DOL-LiTFSI and 0.5 mM DOL-$Al(OTf)_3$ solution. A pre-polymerized DOL electrolyte was then acquired by diluting the DOL-$Al(OTf)_3$ electrolyte with an equivalent volume ratio of DOL-LiTFSI solution.

CR2016-type coin cells were assembled using the Li anode, followed by sequently

adding Celgard 2500, LLTO slice, 200 μL of the pre-polymerized electrolyte solution, and the $LiFePO_4$ cathode or Li metal anode. The entire battery assembly process lasted for 12 h to wait for the complete polymerization of the pre-polymerized PDOL. The in-situ polymerized PDOL/LLTO electrolyte was named In-situ PLE. It should be stressed that the composition of In-situ and Ex-situ electrolytes was identical, except for the way of battery assembly. For comparison, the prepolymer electrolyte solution was also dripped uniformly onto the Teflon substrate and left to stand for 12 h to ensure that the polymerization was complete. The as-obtained polymer electrolyte named as Ex-situ PLE was then stripped from the Teflon substrate for cell assembly. Among them, $LiFePO_4$ was prepared by a slurry coating method. The slurry was composed of $LiFePO_4$ (80 wt%), super P (10 wt%), polyvinylidene fluoride (10 wt%) and *N*-methylpyrrolidone solvent. Then, the uniformly mixed slurry was coated on a carbon-coated aluminum foil, and dried in a vacuum oven at 60 °C for 12 h to completely volatilize the solvent. The active material loading was about 3 mg cm^{-2}.

Material characterizations

The morphology was characterized by field-emission scanning electron microscope (FESEM, JSM 7500F). Transmission electron microscope (TEM, Talos F200S) was used to analyze the electron diffraction of LLTO electrolyte with an energy dispersive spectrometer (EDS) to show the surface element composition distribution. X-ray diffraction (XRD, Bruker AXS D2 Phaser) was used to obtain the crystal structure of LLTO. The pore size distribution of the nanofiber membrane was obtained by a Capillary flow pore size analyzer (PMI, CFP-1500AEX). Thermogravimetry analysis (TG, NETZSCH, TG209 F1 Libra) and differential scanning calorimeter (DSC, TA 4000) were measured at a ramp rate of 5 °C min^{-1} under an N_2 atmosphere. Nitrogen adsorption/desorption isotherms were determined by using a Quantachrome adsorption instrument, and the specific surface area of LLTO electrolyte was calculated by Brunauer-Emmett-Teller (BET). Liquid LiTFSI-DOL and solid PDOL electrolyte were dissolved in dimethyl sulfoxide-d_6 for nuclear magnetic resonance spectrometer analysis (NMR, AVANCE IIITM HD 600MHz). The molecular weight was recorded

by a gel permeation chromatography (GPC). Fourier infrared spectroscopy (FTIR, Nicolet 6700, USA) was conducted using the attenuated total reflection mode to analyze the polymerization process of PDOL. X-ray photoelectron spectroscopy (XPS, Thermo Scientific ESCALAB 250Xi equipped with Al, K_α source) was used to obtain the composition distribution of SEI on the surface of lithium metal after cycling.

Electrochemical measurements

All the electrochemical performance tests (such as galvanostatic discharge/charge profiles, cycling and rate capability) were conducted under a constant temperature environment of 28-30 ℃ using a LAND test system (CT2001A). Linear sweep voltammetry (LSV), chronoamperometry (IT), electrochemical impedance spectroscopy (EIS) and ion conductivity tests were all performed on an electrochemical workstation (CHI660C).

The electrochemical stability window was measured by the linear sweep voltammetry (LSV). The measurements were collected with the Li foil as the counter electrode and the stainless-steel disc as the working electrode. The assembled cell was tested at a scan rate of 0.1 mV s^{-1} with a voltage of 1-6 V (vs. Li^+/Li).

The Li^+ transference number (t_{Li^+}) was measured with chronoamperometry by using a Li|Li symmetric cell at a constant step potential (ΔE) of 10 mV. The specific values were calculated according to the following equation:[1]

$$t_{Li^+} = \frac{I^{ss}R_b^{ss}\left(\Delta E - I^0 R_i^o\right)}{I^0 R_b^0\left(\Delta E - I^{ss}R_i^{ss}\right)} \#() \quad (1)$$

where I^{ss} and I^0 represent the steady-state and initial-state currents, respectively. The initial and steady-state values of the bulk resistances (R_b^0 and R_b^{ss}) and interfacial resistances (R_i^o and R_i^{ss}) were examined before and after the potentiostatic polarization via EIS.

The interfacial impedance and ion conductivity of Li|Li cells were measured by electrochemical impedance spectrometry (EIS) tests in a frequency range from 100 kHz to 0.1 Hz. Moreover, the ion conductivity tests were also performed at 0 ~ 50 °C and calculated according to the following equation:[2]

$$\sigma = \frac{L}{R \times S} \#() \quad \textbf{2.}$$

where σ is the ion conductivity, L is the membrane thickness, R is the impedance and S is the contact area. The activation energy (E_a) of the polyether-based composite electrolyte was calculated by Arrhenius relationship:[3]

$$\sigma = Ae^{\frac{-E_a}{RT}} \#(3)$$

where T is the absolute temperature, A is the pre-exponential factor, E_a is the activation energy and R is the universal gas constant of 8.314 J mol^{-1}.

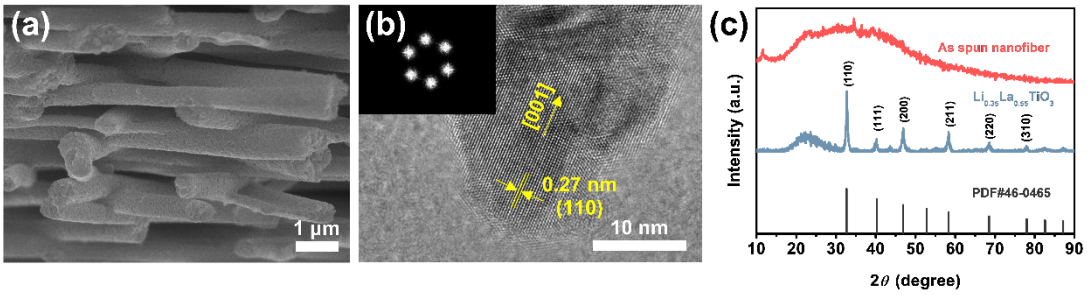

Fig. S1 Characterizations of the LLTO NF membrane. (a) Cross-sectional SEM image; (b) HRTEM image of an individual LLTO NF and the inset is the corresponding FFT pattern; (c) XRD patterns.

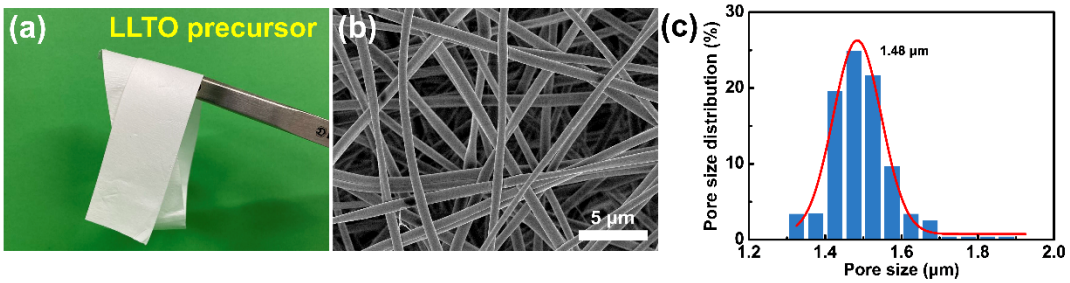

Fig. S2 The flexible precursor membrane prepared by electrospinning: (a) bending photograph, (b) SEM image, and (c) pore size distribution.

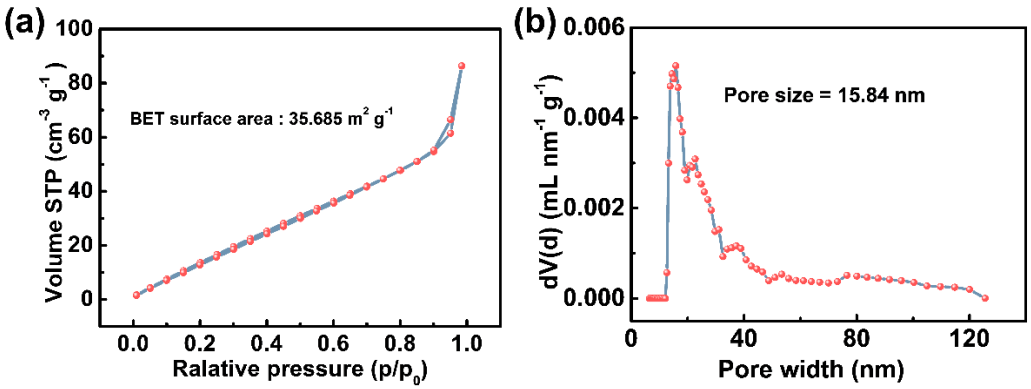

Fig. S3 (a) N_2 adsorption-desorption isotherms and (b) the pore size distribution of LLTO NFs.

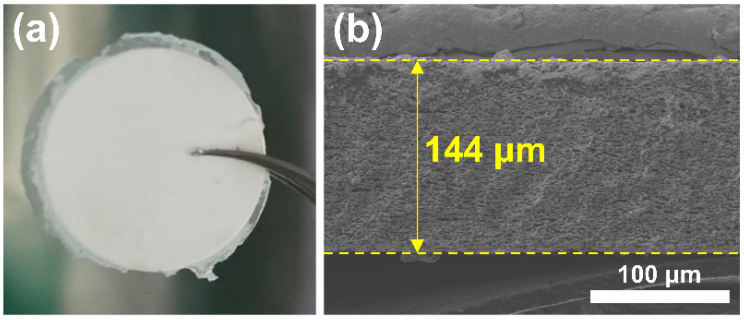

Fig. S4 (a) The digital photograph and (b) cross-sectional image of PLE electrolyte with a controlled thickness.

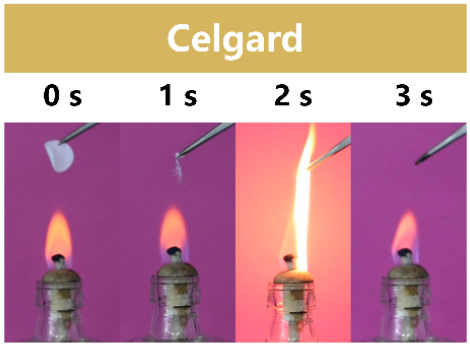

Fig. S5 Combustion test photographs of the Celgard separator.

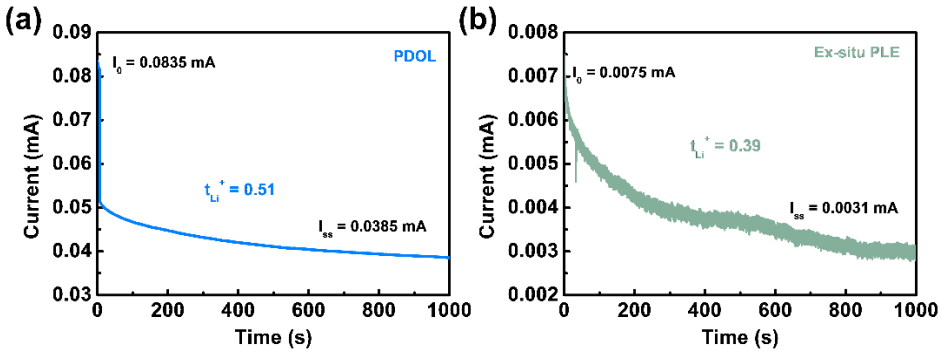

Fig. S6. Current–time curves of (a) PDOL and (b) EX-situ PLE at 10 mV following DC polarization.

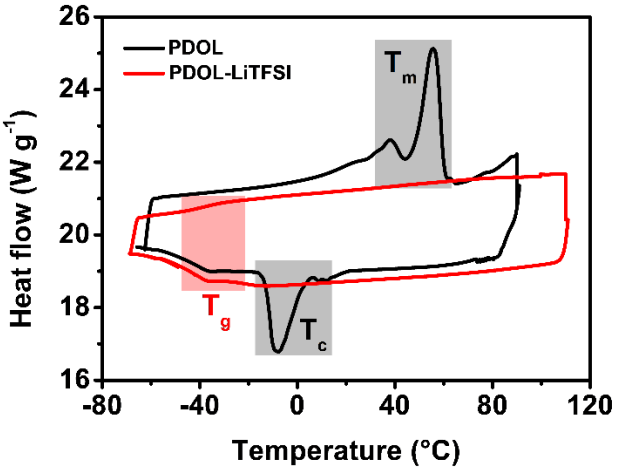

Fig. S7 DSC analyses of PDOL with and without LiTFSI.

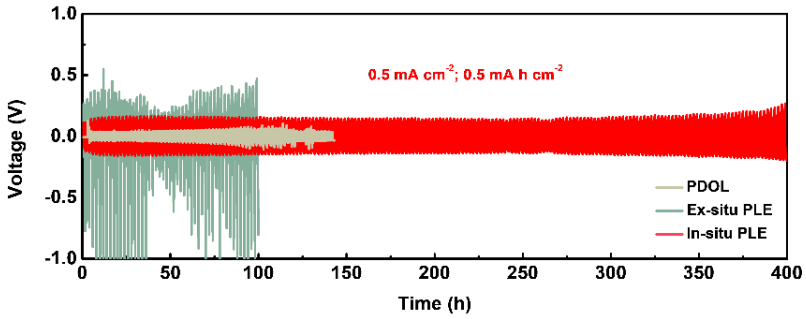

Fig. S8 Cycle stabilities of Li|Li symmetric cells at a current density of 0.5 mA cm^{-2}.

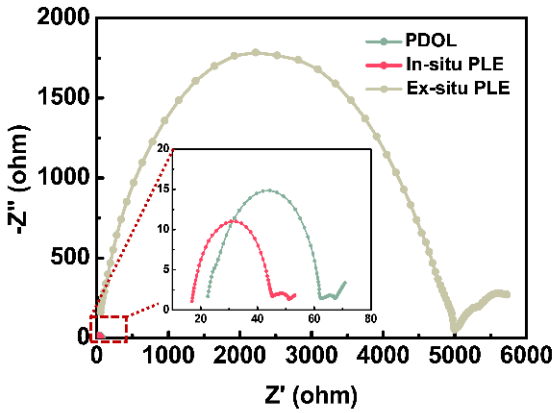

Fig. S9 EIS tests of the Li|Li symmetric cells carried out before cycling.

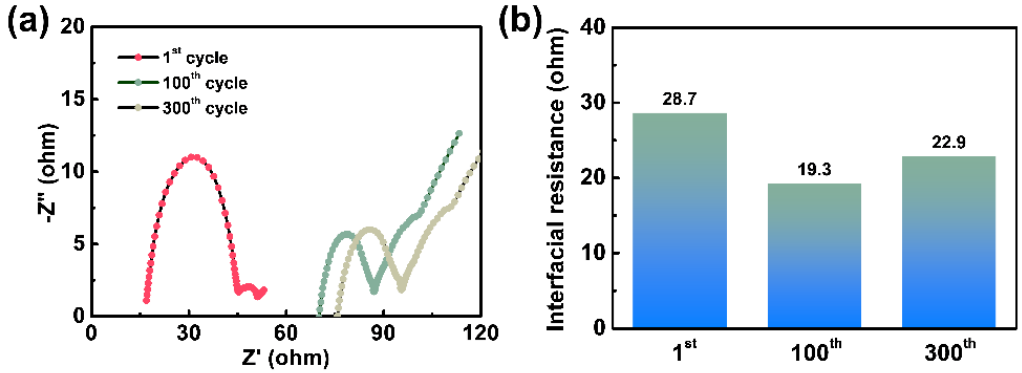

Fig. S10 (a) EIS analyses at different cycles and (b) the corresponding interfacial resistance (R_{ct}) in the Li|In-situ PLE|Li symmetric cells.

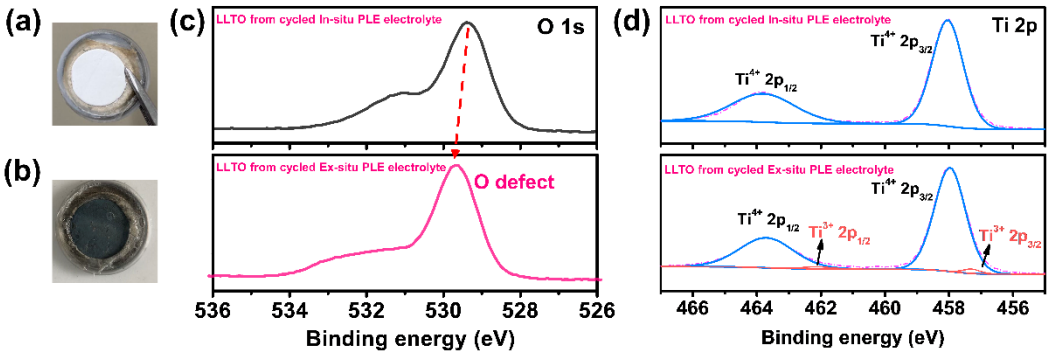

Fig. S11 (a, b) Digital photographs of the white LLTO and black LLTO. XPS spectra of (c) O 1s and (d) Ti 2p of the cycled In-situ PLE and Ex-situ PLE electrolytes in the Li|Li symmetric batteries.

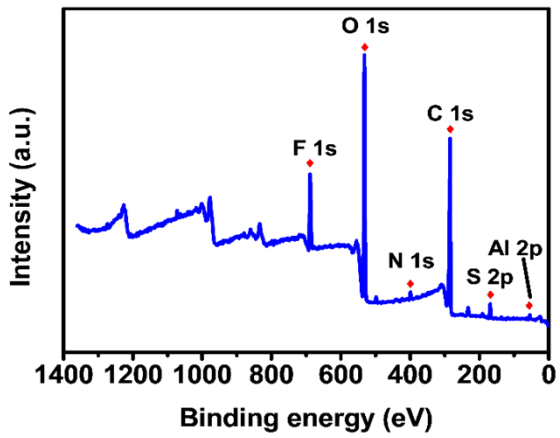

Fig. S12 The XPS full spectrum of the Li metal disassembled from Li|In-situ PLE|Li

cell after 5th cycle.

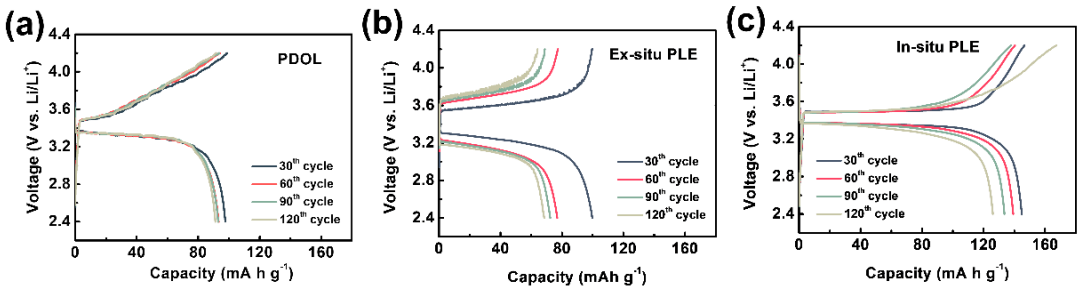

Fig. S13 Galvanostatic charge–discharge curves of (a) Li|PDOL|LFP, (b) Li|Ex-situ PLE|LFP and (c) Li|In-situ PLE|LFP full batteries, respectively.

References

1 W. Xiao, K. Y. Zhang, J. G. Liu, C. W. Yan, *J. Mater. Sci. Mater. Electron.*, 2017, **28**, 17516–17525.

2 Y. Cao, C. Liu, M. D. Wang, H. Yang, S. Liu, H. L. Wang, Z. X. Yang, F. S. Pan, Z. Y. Jiang, J. Sun, *Energy Storage Mater.*, 2020, **29**, 207–215.

3 J. Sun, C. He, X. Yao, A. Song, Y. Li, Q. Zhang, C. Hou, Q. Shi, H. Wang, *Adv. Funct. Mater.*, 2020, **31**, 2006381.